J. Fluid Mech. (1978), *vol.* 87, *part* 1, *pp.* 121–141
Printed in Great Britain

A turbulent boundary layer disturbed by a cylinder

By EISUKE MARUMO, KENJIRO SUZUKI AND TAKASHI SATO

Department of Mechanical Engineering,
Kyoto University, Kyoto, Japan

(Received 1 January 1977 and in revised form 29 September 1977)

This paper deals with a two-dimensional turbulent boundary layer disturbed by a circular cylinder. The cylinder was placed inside or outside the boundary layer with its axis parallel to the wall and normal to the flow direction. The mean velocity, wall shear stress, longitudinal turbulent intensity, autocorrelations and turbulent length scale were measured and here the relaxation features of the disturbed boundary layer are discussed. The measurements were made for a ratio of the cylinder diameter d to the undisturbed boundary-layer thickness δ_0 equal to 0·30 and for three values of the ratio of the height h of the cylinder axis to δ_0 equal to 0·222, 0·556 and 1·24.

The results show that the near-wall region of the disturbed boundary layer recovers much more quickly than the outer region and that in the case $h/\delta_0 = 0{\cdot}222$ the recovery is faster than in other cases, as reported by Clauser (1956). Moreover, it is found that the fluctuating velocity field recovers more slowly than the mean velocity field, and that the characteristics of the turbulence in the outer region are still close to those in the wake of an isolated cylinder at the last measurement station, although the mean velocity profile has almost completely returned to its natural shape.

1. Introduction

Up to the present time, studies of turbulent boundary layers have related mainly to perturbations of surface conditions, such as surface roughness, or of mainstream conditions, such as the free-stream turbulence. Little work has been done on the effect of perturbations within the boundary layer.

The present study deals with a turbulent boundary layer disturbed by a cylinder mounted with its axis spanwise at some distance from the surface. This type of flow is intermediate between boundary-layer flow affected by free-stream turbulence and boundary-layer flow developed over a rough surface.

A cylinder placed in a boundary layer will produce distortion of the mean velocity profile and agitate the fluctuating velocity field. As the boundary layer proceeds downstream, the distortion and excess fluctuations decay and the disturbed boundary layer returns to its natural shape. This relaxation process involves an interaction between the wall turbulence and the newly generated wake-like turbulence. For different values of d/δ_0, h/δ_0 and the mainstream velocity U_∞, the distortion and the fluctuating field seem to have different characteristics, and various types of relaxation process may arise.

For these reasons, this flow is suitable for checking the applicability or generality

of the recent mathematical turbulence models and also for investigation of the wall turbulence mechanism or the mechanism of turbulent heat transfer.

To the authors' knowledge, the only previous papers on this subject are those of Clauser (1956), Eskinazi (1958) and, recently, Fujita, Takahama & Yamashita (1974). Clauser did the pioneering work on this flow and measured the mean velocity distributions downstream of the cylinder. In his study, the measurements were carried out for $d/\delta_0 = 0{\cdot}054$ and for $h/\delta_0 = 0{\cdot}16$ and $0{\cdot}59$. He found that the inner portion of the boundary layer returned much more quickly to the universal profile than did the outer portion. Eskinazi measured the mean velocity, turbulence intensity, static pressure and turbulence length scale in a fully developed channel flow disturbed by a cylinder and discussed the decay of the cylinder wake. Here d/D was $0{\cdot}0127$ (D being the channel width) and h/D ranged from $0{\cdot}072$ to $0{\cdot}5$. Fujita *et al.* carried out heat-transfer measurements along the wall downstream of the cylinder and found that heat transfer can be promoted by the insertion of a cylinder. In their measurements, U_∞ was about 20 m/s, d/δ_0 was $0{\cdot}57$ and h/δ_0 ranged from $0{\cdot}28$ to $6{\cdot}0$. As indicated above, Clauser and Eskinazi chose much smaller values of d/δ_0 (or d/D) than did Fujita *et al.* and the present authors. In view of these studies, further detailed investigations were considered necessary in order to clarify the features of the flow. Therefore the present authors have attempted experimental and theoretical studies of the flow.

Other studies of disturbed boundary layers are those reviewed by Tani (1968) and the more recent studies of the flow after a step (Bradshaw & Wong 1972), a turbulent wall jet in a moving stream (Kacker & Whitelaw 1968, 1971), the flow after a hemispherical cap on a wall (Hinze, Sonnenberg & Builtjes 1974), the flow over a surface changing from rough to smooth (Antonia & Luxton 1972) and the flow on a slotted flap (Irwin 1974). Most of these discussed the applicability of the turbulence models from their viewpoints. Kacker & Whitelaw also carried out detailed measurements of the mean and fluctuating properties of the wall jet for an average slot velocity less than the free-stream velocity. It is of interest that the characteristics of these properties resemble those obtained in the present investigation.

This paper presents the results of some measurements of the mean and fluctuating velocity field and discusses the relaxation of the disturbed boundary layer.

2. Experimental apparatus and procedures

The wind tunnel used in this study, shown schematically in figure 1, is an open-circuit one which consists of a honeycomb flow straightener and two screens followed by a 9 : 1 contraction chamber, a 38×38 cm test section and a driving fan. The test boundary layer developed on a smooth flat plate from its leading edge, which was located 262 cm downstream from the outlet port of the contraction chamber. The flat plate was used as the lower wall of the tunnel, the floor boundary layer being sucked off at the leading-edge position. The suction velocity was adjusted, prior to the measurements, to ensure uniformity of the main flow at the leading edge. The first 40 cm of the plate was covered by sandpaper for the purpose of tripping the boundary layer. The upper wall of the tunnel was made in such a shape as to give a zero pressure gradient in the tunnel, the residual variation of the static pressure being less than $0{\cdot}2$ % of the main-flow dynamic pressure, except for an unavoidable step-like change at the

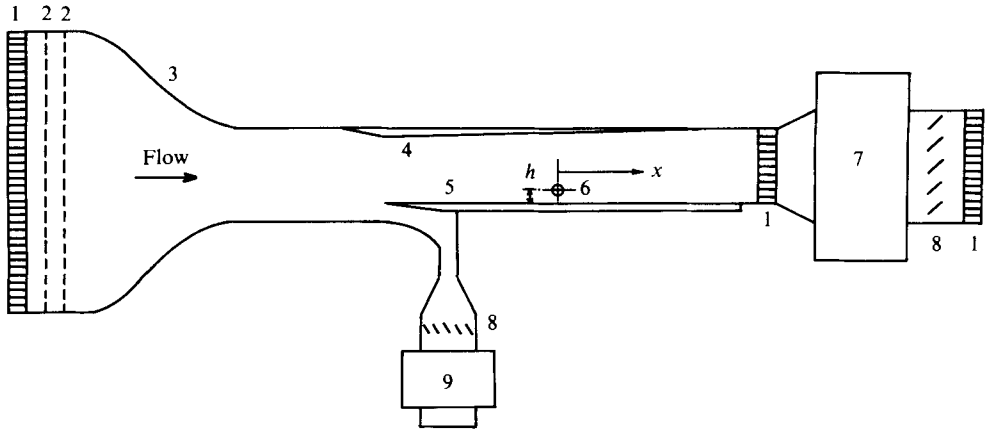

FIGURE 1. Sketch of test arrangement. (1) Honeycomb. (2) Screen. (3) Contraction chamber. (4) Upper wall. (5) Test plate. (6) Circular cylinder. (7) Main blower. (8) Flow controller. (9) Suction blower.

position of the cylinder. The relative intensity of the mainstream turbulence was less than 0·9 % at the test mainstream velocity of 14 m/s.

A cylinder of diameter 0·8 cm was used for the experiment. The streamwise location of the cylinder was fixed at 140 cm downstream from the leading edge. The thickness of the undisturbed boundary layer was 2·7 cm at this station. The space between the cylinder axis and the wall was set at three different values, the locations h of the cylinder axis being 0·60, 1·50 and 3·35 cm above the wall. These three positions correspond roughly to positions very near the inner layer, in the middle of the outer layer and just outside the boundary layer. The majority of the measurements were made at six stations 3·7, 8·7, 18·7, 38·7, 63·7 and 83·7 cm downstream from the cylinder.

Separate Pitot–static tubes were used for the measurement of static pressure and mean velocity, and as Preston tubes. Both tubes were made of stainless-steel pipe of outer diameter 0·12 cm and inner diameter 0·06 cm, and the gap between the two tubes was chosen to avoid interference effects on the reading. This probe was calibrated against a standard Prandtl-type probe and its accuracy of velocity measurement was within 0·7 %. Surface shear stresses were derived from the reading of a surface Pitot tube with the aid of Patel's (1965) calibration curve. The mean velocity profiles and turbulence properties were measured with a single hot wire (a 5 μm diameter tungsten wire 1 mm long) and a constant-temperature anemometer. The output voltage of the anemometer E was electronically linearized in accordance with the relation

$$U = \left(\frac{E^2 - A}{B}\right)^2, \tag{1}$$

where the constants A and B were determined from the hot-wire calibration. In the case of the autocorrelation measurements the linearized signal was recorded on a magnetic tape recorder and processed with a digital correlator.

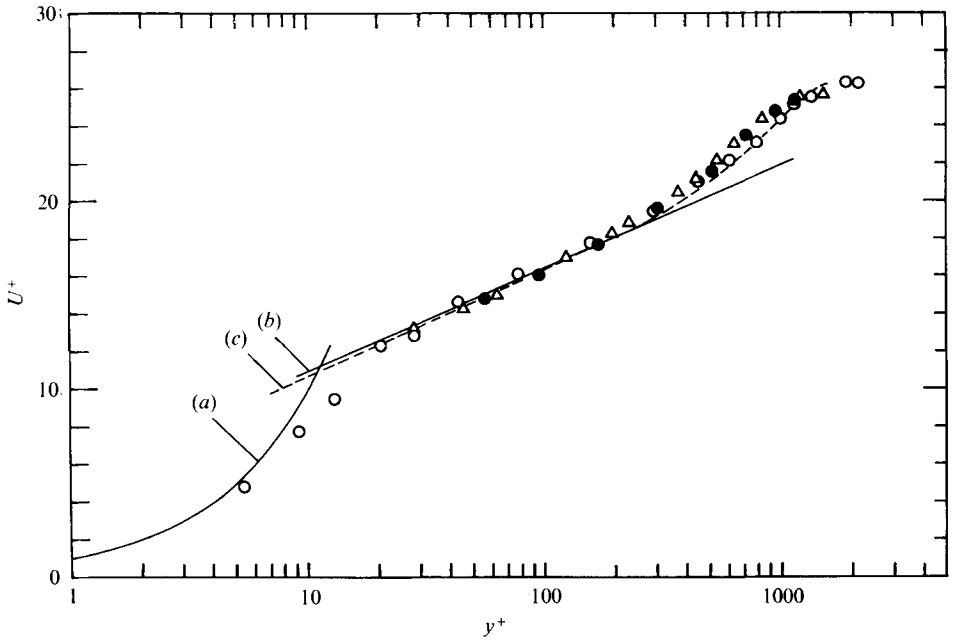

FIGURE 2. Logarithmic velocity distributions for the undisturbed boundary layer. ●, x = 3·7 cm; △, x = 18·7 cm; ○, x = 83·7 cm. (*a*) Equation (2). (*b*) Equation (3). (*c*) Equation (4).

3. Preliminary experiments

In this section the results of preliminary measurements of an undisturbed turbulent boundary layer and the wake of an isolated cylinder are described. The profiles of the mean velocity measured in the boundary layer are shown in figure 2 on a semi-logarithmic plot. The friction velocity U_τ was derived from Preston-tube measurements. The solid curve (*a*) and the line (*b*) in the figure may be expressed as follows:

$$U^+ \equiv U/U_\tau = yU_\tau/\nu \equiv y^+, \tag{2}$$

$$U^+ = 5{\cdot}5 \log y^+ + 5{\cdot}45, \tag{3}$$

where y is the distance from the wall and ν is the kinematic viscosity of the fluid. Equation (3) is the logarithmic law given by Patel (1965). The measured velocity is in good agreement with (3) in the logarithmic region.

Coles (1968) provided the following universal velocity profile for the outer layer:

$$U^+ = 5{\cdot}62 \log y^+ + 5{\cdot}0 + 2{\cdot}44 \Pi w(y/\delta), \tag{4}$$

where Π is a parameter representing the strength of the wake component,

$$w(y/\delta) = 2 \sin^2 (\pi y/2\delta)$$

and δ is the boundary-layer thickness. Coles carefully chose the values of the parameters U_τ, δ and Π by searching for the best fit of (4) with the data and by using the relation

$$U_\infty/U_\tau = 5{\cdot}62 \log (\delta U_\tau/\nu) + 5{\cdot}0 + 2{\cdot}44 \Pi w(1), \tag{5}$$

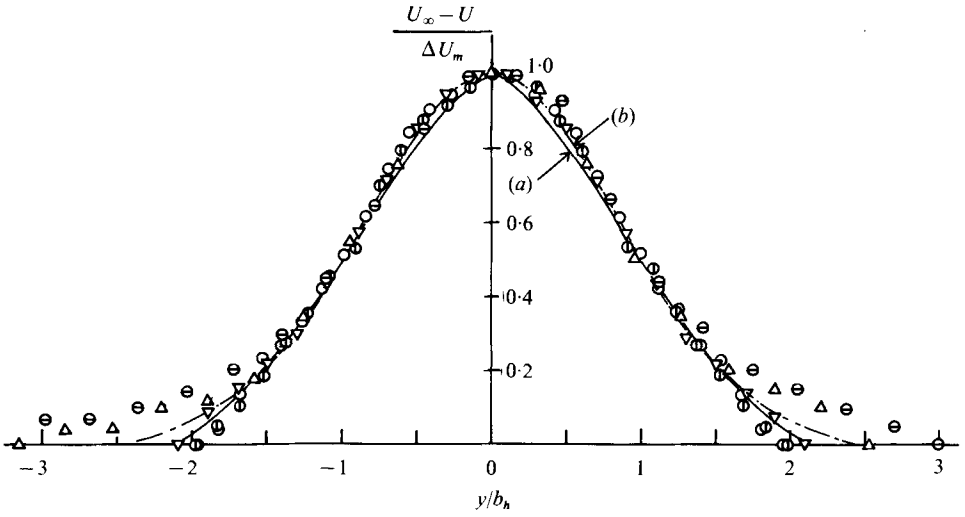

FIGURE 3. Velocity profiles for the wake. ⊖, $x/d = 11$; △, $x/d = 23{\cdot}4$; ▽, $x/d = 48{\cdot}4$; ①, $x/d = 79{\cdot}6$; ○, $x/d = 105$. (*a*) Equation (6). (*b*) Equation (6*a*).

which is obtained simply by setting $y = \delta$ and $U = U_\infty$ in (4). This indirect method is not adopted in the present study. Instead, the following convenient method is used to determine the values of the three parameters: the friction velocity U_τ is derived from Preston-tube measurements, the boundary-layer thickness δ is taken as the distance to the point where $U/U_\infty = 0{\cdot}99$ in the measured velocity profile, while the remaining parameter Π is determined by substituting the values of U_τ and δ into (5). Careful comparison between the two methods for some available data (Coles 1968) shows that the present method generates velocity profiles slightly higher (by about 0·4 for U^+) than those obtained by the method of Coles and that the value of Π is higher than that determined by Coles by about 0·05 for the case $U_\infty^+ = 25$. The broken curve in figure 2 is the velocity profile generated in this way which corresponds to the measured profile at $x = 83{\cdot}7$ cm. The value of Π for this case is 0·666.

The relative intensity of the streamwise fluctuating velocity was also measured and the results are in good agreement with the profile given by Klebanoff (1954). They are not shown here but are used in the discussion in the next section.

Figure 3 shows the velocity distributions in the wake of a circular cylinder. The Reynolds number $U_\infty d/\nu$ based on the cylinder diameter d was $7{\cdot}65 \times 10^3$ in this experiment. The results at $x/d \geqslant 48$ are in good agreement with the following profiles given by Schlichting (1930) and Reichardt (1942), respectively:

$$(U_\infty - U)/\Delta U_m = [1 - (0{\cdot}441 y/b_h)^{\frac{3}{2}}]^2, \tag{6}$$

$$(U_\infty - U)/\Delta U_m = \exp[-(0{\cdot}8375 y/b_h)^2], \tag{6a}$$

where $\Delta U_m = U_\infty - U_0$ is the maximum velocity defect, U_0 the fluid velocity at the centre of the wake, y the distance from the centre-plane of the wake and b_h the half-width of the wake. The drag coefficient of the cylinder calculated from the velocity distributions at $x/d = 105$ was 0·973, a little smaller than that obtained by Wieselsberger (see Schlichting 1968, p. 17). The streamwise variations of the wake half-width and maximum velocity defect are expressed by $b_h = 0{\cdot}693\sqrt{x}$ and $\Delta U_m = 38{\cdot}3/\sqrt{x}$,

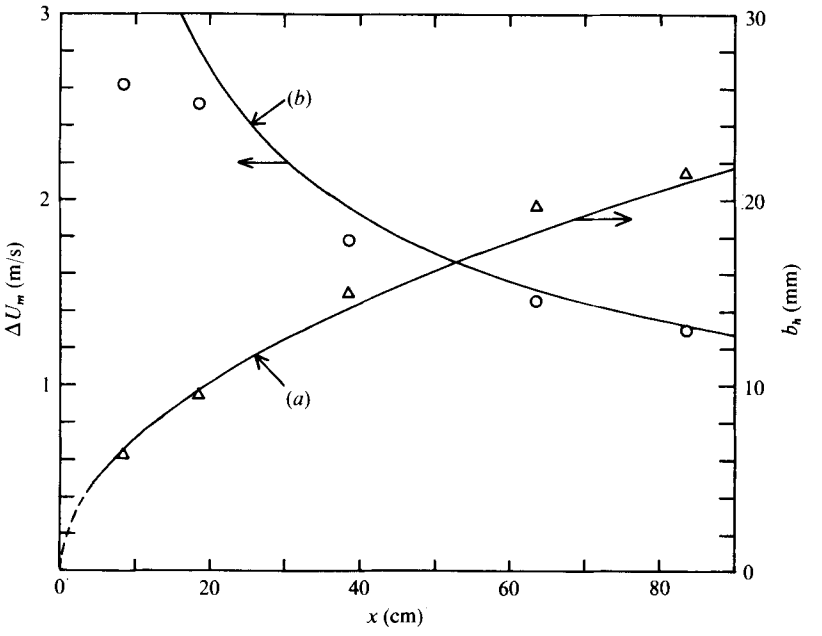

FIGURE 4. Variation of b_h and ΔU_m with x.
△, b_h; ○, ΔU_m. (*a*) $b_h = 0{\cdot}693\sqrt{x}$. (*b*) $\Delta U_m = 38{\cdot}3/\sqrt{x}$.

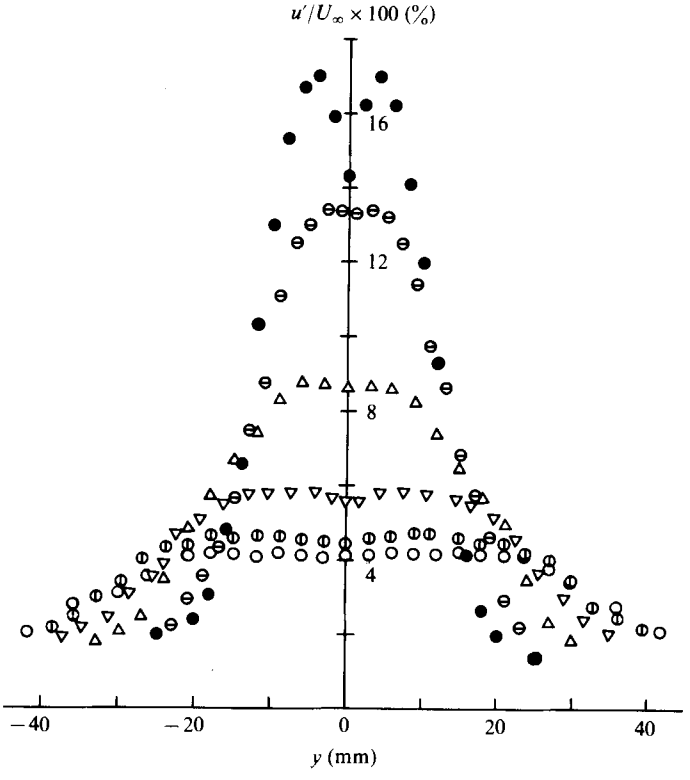

FIGURE 5. Distributions of longitudinal turbulence intensity for the wake.
●, $x/d = 4{\cdot}6$; other symbols as in figure 3.

respectively, from the formulae given by Schlichting using the above value of the drag coefficient. Here x is measured in millimetres. These relationships are compared with the experimental results in figure 4. Significant differences can be seen between the measured values of ΔU_m and the above relationship for the far wake, but the variation in the half-width follows the far-wake relationship relatively well. The relative intensity of the streamwise fluctuating velocity found in the wake is shown in figure 5.

The autocorrelation of the streamwise fluctuating velocity was obtained in the wake and transformed into the spatial correlation using Taylor's hypothesis. The results obtained at $x = 3{\cdot}7$ cm, rather close to the cylinder, are shown in figure 12(a). The contribution of Kármán vortices to the velocity fluctuation is found to be significant at $x/d = 4{\cdot}6$, and even at $x/d = 23{\cdot}4$ (not shown here), the periodic component of the velocity fluctuation due to the vortices contributes about 10 % of the intensity of the streamwise velocity fluctuation, according to a simple estimate based on the assumption that the periodic component contributes independently to the correlation. The frequency of the periodic fluctuation was about 325 Hz except in the central part of the wake, where the frequency was doubled, and the Strouhal number corresponding to the frequency was about 0·185. Figure 13(a) shows the distribution of the integral length scale of the wake calculated from the transformed space correlation according to the definition†

$$L_x = \int_0^\infty R_{uu}(r, 0, 0)\, dr = \int_0^\infty \frac{\overline{uu(r)}}{\overline{u^2}}\, dr, \tag{7}$$

where r denotes the distance deduced from the time interval using Taylor's hypothesis. The integral scale L_x for an undisturbed boundary layer is also shown in the figure. The quantity $\bar{L}_x$ shown in the figure is the average of L_x over the entire cross-section of the wake or over the outer layer of the undisturbed boundary layer. The length scale $\bar{L}_x$ at $x/d = 23{\cdot}4$ in the wake is about 8 mm, which is about one-third of that in the undisturbed boundary layer at the same location. The two values of the length scale, however, become close to each other at the station $x/d = 105$ because the length scale increases more rapidly with x in the wake than in the boundary layer.

4. Experimental results and discussion

This section gives the experimental results for the three disturbed boundary layers mentioned above. These results include the streamwise distribution of the skin-friction coefficient, the profiles of mean velocity and turbulence intensity, and the correlation coefficient and length scale of turbulence. In addition, some features of the relaxation process in the boundary layer are described.

Figure 6 shows the skin-friction coefficient c_f evaluated from the reading of the Preston tube. The way in which c_f varies in the streamwise direction differs remarkably for different values of h. In the case $h = 0{\cdot}60$ cm, c_f is very small just after the cylinder but increases rapidly with the increasing distance downstream. The very small value

† Measurements not shown here indicated that the autocorrelation decayed with increasing time interval t even when strong periodicity was found. For such cases, the integral length scale was determined by integrating over the first few periods. This value is not correct in the strict sense but may be considered here to be roughly equal to $\int_0^\infty R_{uu}\, dt$.

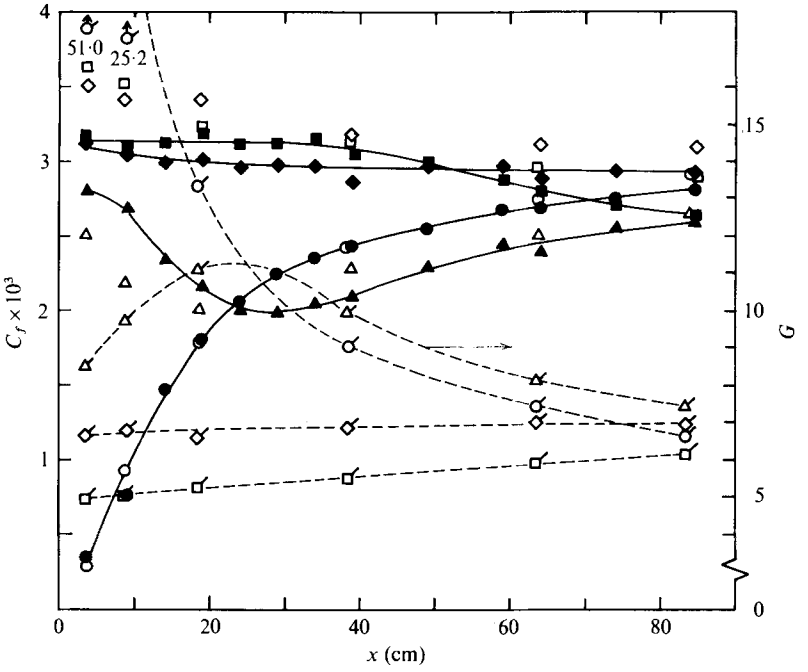

FIGURE 6. Variation of the skin-friction coefficient and the Clauser parameter G with x. ◇, undisturbed; ○, $h = 0{\cdot}60$ cm; △, $h = 1{\cdot}50$ cm; □, $h = 3{\cdot}35$ cm. Open symbols, c_f from Ludwieg & Tillmann's formula (8); closed symbols, present experiments; flagged symbols, G.

of c_f observed suggests that a small recirculating bubble exists on the wall close to the cylinder. When $h = 3{\cdot}35$ cm, c_f remains almost constant up to $x = 40$ cm then decreases slowly with increasing x. This may correspond to the fact, which will be established later, that the wake turbulence does not come close to the wall at small values of x because there is a rather large gap between the wall and the cylinder. When $h = 1{\cdot}50$ cm the c_f variation is intermediate between the two cases given above. The effect of cylinder appears just after the cylinder, and reduces the value of c_f with increasing x. The greatest effect appears at $x = 30$ cm and the restoration starts thereafter. These observations show that the effect of the cylinder is composed of the direct effect of the induced change in flow pattern and the indirect effect of the arrival of wake turbulence at the wall. The former effect is weak when $h = 3{\cdot}35$ cm but it is somewhat larger when $h = 1{\cdot}50$ cm. The latter suggests that the turbulence outside the boundary layer, or the free-stream turbulence, penetrates deep enough to affect the skin friction and the heat transfer from the wall if the turbulence is strong.

The Preston tube was used with the intention of finding the qualitative nature of the flow near the wall. As will be shown later, the profiles of the mean velocity near the wall appear to obey the law of the wall (with a friction velocity evaluated from the reading of the Preston tube) except at the x stations just after the cylinder. Moreover, the extrapolations to the wall of the lateral turbulent shear-stress profiles (to be reported later) coincide almost perfectly with the above values at x stations not too close to the cylinder. Figure 6 also shows the values of c_f calculated from an empirical relation

$$c_f = 0{\cdot}246 \times 10^{-0{\cdot}678 H_{12}} (U_\infty \delta_m / \nu)^{-0{\cdot}268} \tag{8}$$

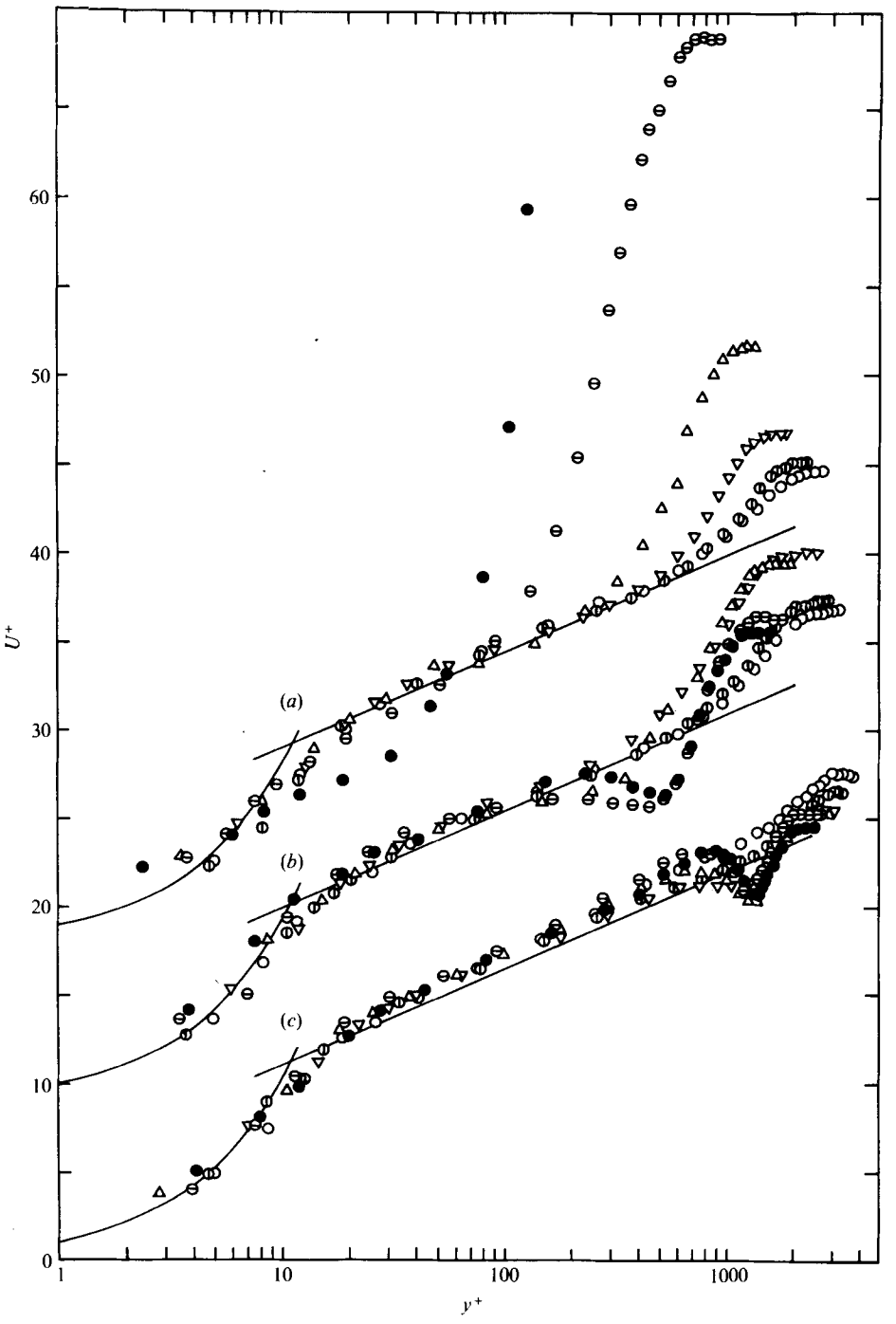

FIGURE 7. Logarithmic velocity distributions for the disturbed boundary layers. (*a*) $h = 0{\cdot}60$ cm. (*b*) $h = 1{\cdot}50$ cm. (*c*) $h = 3{\cdot}35$ cm.

	●	⊖	△	▽	⊙	○
x (cm)	3·7	8·7	18·7	38·7	63·7	83·7
x/d	4·6	11	23·4	48·4	79·6	105

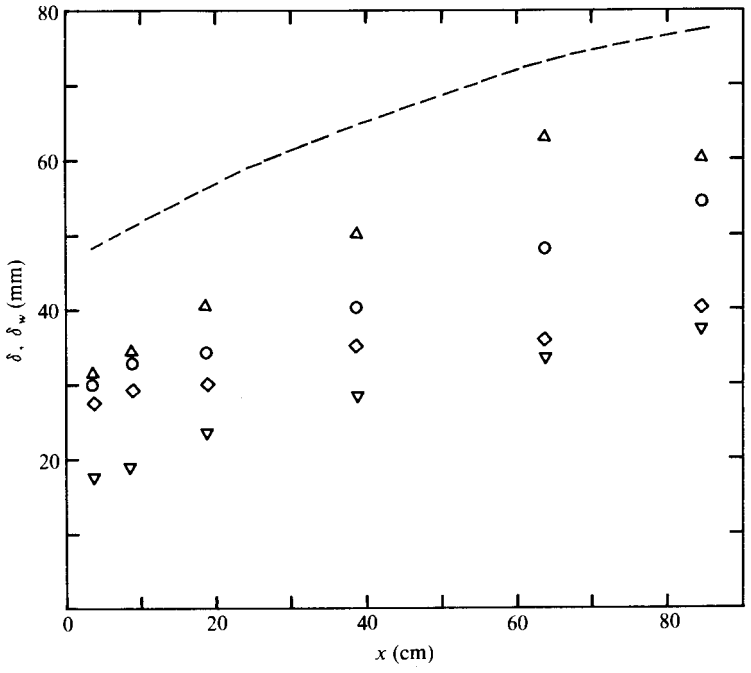

FIGURE 8. Variation of the thicknesses of the boundary layer and wake.
◇, undisturbed; ○, h = 0·60 cm; △, h = 1·50 cm; ---, h = 3·35 cm; ▽, wake.

given by Ludwieg & Tillmann (1950). Here δ_m is the momentum thickness, $H_{12} = \delta_d/\delta_m$ is the shape factor and δ_d is the displacement thickness. These were calculated from the mean velocity profiles. The discrepancy between measured and calculated values of c_f is not very large. Another empirical formula, given by Escudier, Nicoll & Spalding (1966), was also evaluated. The results are almost the same as those given by (8) except that they are consistently lower by about 0·0003, on average, for all three cases. This indicates that these empirical formulae are useful for the rough estimation of c_f even in the present kind of strongly disturbed boundary layer.

Figure 7 shows a logarithmic plot of the mean velocity measured at several x stations, the friction velocity being that obtained from the Preston-tube measurements. All the profiles seem roughly to obey the logarithmic profile (3) after x = 18·7 cm. (The absence of a region obeying (3), of course, implies unreliability of the Preston tube, which relies on the law of the wall.) This shows that the recovery of the flow pattern from the disturbance is fairly rapid near the wall. It also indicates that the flow in the region of the logarithmic law is strongly restricted by the local wall shear stress even in the present relaxing flow. In the cases h = 1·50 and 3·35 cm a depression is still visible after the flow near the wall again obeys the logarithmic law. This suggests that it takes longer for the outer than for the inner part of the boundary layer to readjust or to relax. In connexion with this, it is noticed that the rapid decrease in the wake component in the case h = 0·60 cm is merely a reflexion of the rapid increase in c_f and the fast readjustment of the velocity distribution in the inner layer, because the actual value of the velocity does not vary so rapidly with increasing x in the outer layer.

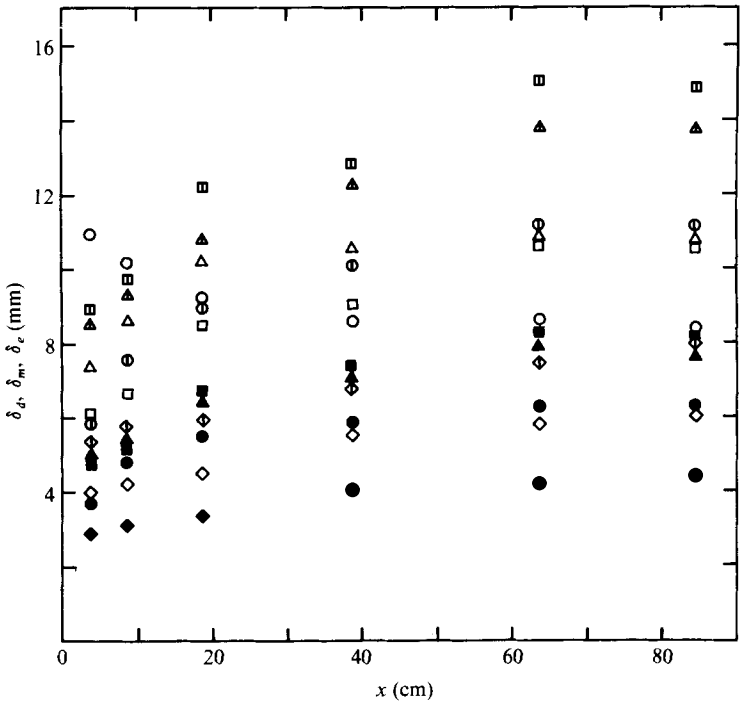

FIGURE 9. Variation of integral thicknesses with x.

		δ_d	δ_m	δ_e
h =	0·60 cm	○	◐	●
	1·50 cm	△	◬	▲
	3·35 cm	□	▣	■
Undisturbed		◇	◈	◆

In figure 8 the development of the boundary-layer thickness δ is compared with that of the cylinder wake. The latter is defined as the distance δ_w from the central plane to the point where the mean velocity defect is 1 % of the free-stream velocity for consistency with the definition of the boundary-layer thickness. When $h = 3{\cdot}34$ cm, δ is defined as the distance from the wall to the position where $U/U_\infty = 0{\cdot}99$. This is shown by a dotted line in the figure. In this case δ does not necessarily indicate the region of the wall turbulence. As seen in the figure, the growth rate of the disturbed boundary layer differs somewhat from that of the undisturbed boundary layer but is similar to that of the cylinder wake. This indicates that the mechanism of turbulence in the outer part of boundary layer, governing the entrainment rate, remains similar to that of the wake turbulence rather than to that of the wall turbulence over the whole x region observed. This is in agreement with results shown later which suggest that some features of turbulence do not recover as quickly as the mean velocity profile.

Figure 9 shows the variation of other characteristic thicknesses of the boundary layer. The displacement thickness δ_d decreases and increases monotonically with increasing x when $h = 0{\cdot}60$ and $3{\cdot}35$ cm respectively. For the case $h = 1{\cdot}50$ cm, on the other hand, δ_d initially increases with x but begins to decrease after $x = 60$ cm. In figure 10 the results shown in figure 9 are replotted in the form δ_e/δ_m *vs.* δ_d/δ_m.

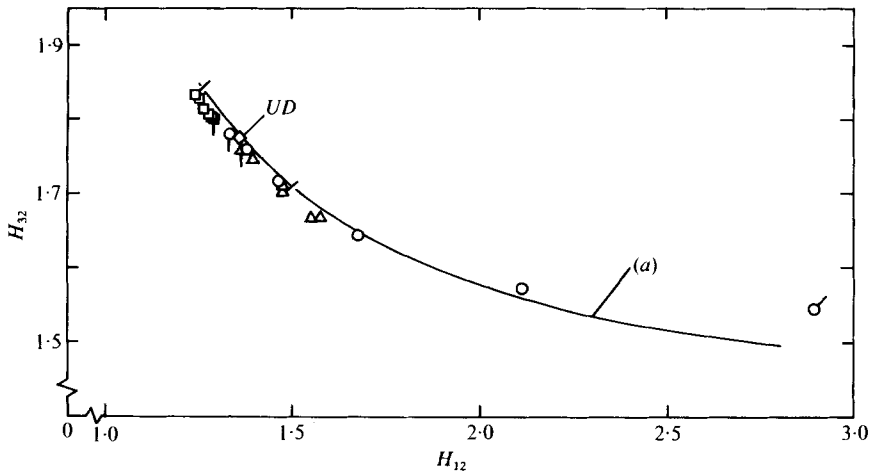

FIGURE 10. Relation between H_{12} and H_{32}. ◇, undisturbed; ○, h = 0·60 cm; △, h = 1·50 cm; □, h = 3·34 cm. Flags: /, x = 3·7 cm; |, x = 83·7 cm. (*a*) Equation (9).

The curve in the figure is the following empirical equation given by Nicoll & Escudier (1966) for a boundary layer which has a velocity peak:

$$H_{32} = 1{\cdot}431 - \frac{0{\cdot}0971}{H_{12}} + \frac{0{\cdot}775}{H_{12}^2}, \quad 2{\cdot}8 > H_{12} \geqslant 1{\cdot}25, \tag{9}$$

where $H_{12} = \delta_d/\delta_m$ and $H_{32} = \delta_e/\delta_m$. The present results agree fairly well with the curve except at x = 3·7 cm in the case h = 0·60 cm. As seen in the figure, the points for h = 3·35 cm do not deviate so much from the point *UD* for the undisturbed boundary layer and do not vary significantly throughout the part of relaxation process observed. In contrast, the initial point for h = 0·60 cm lies fairly far from the point *UD* but the following points rapidly approach to the point *UD*. The final point in the case h = 0·60 cm is much closer to the point *UD* than in the case h = 3·35 cm. This suggests that the restoration rate of the mean velocity profile as a whole is a little faster in the case h = 0·60 cm than in the other cases. Figure 6 also shows the streamwise variation of another parameter G defined by Clauser as

$$G = \left(\frac{2}{c_f}\right)^{\frac{1}{2}} (H_{12} - 1)/H_{12}. \tag{10}$$

The value of G for the present undisturbed case was 6·8 on average, which is the value usually proposed for equilibrium constant-pressure turbulent boundary layers. In the case h = 0·60 cm, the degree of non-equilibrium of the boundary layer decreases rapidly and the value of G becomes smaller than that of the undisturbed boundary layer. When h = 1·50 cm, the value of G initially increases with x then begins to decrease after a location some distance from the cylinder. The variation of G in the case h = 3·35 cm is different from that in the other two cases, G increasing towards the value for the undisturbed case slowly and monotonically with x. This agrees well with the trends in figure 10.

Clauser observed the decay rate of the mean velocity distortion and found that the recovery from the distortion was faster when h was smaller. The same was done in the present study and the results are shown in figure 11. The reference velocity was

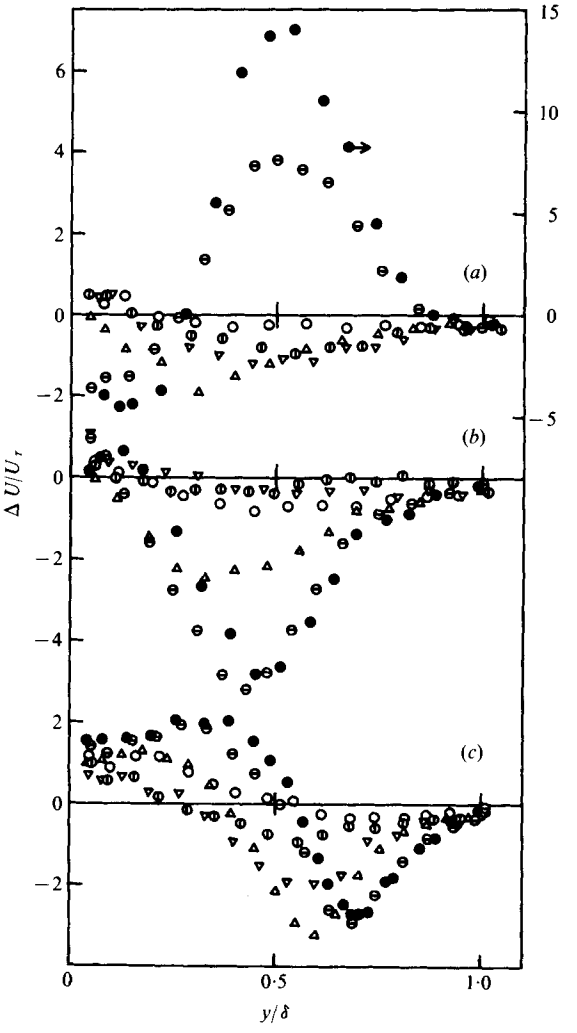

FIGURE 11. Distributions of velocity difference between measured velocity profile and reference one. (*a*) $h = 0{\cdot}60$ cm. (*b*) $h = 1{\cdot}50$ cm. (*c*) $h = 3{\cdot}35$ cm. Symbols as in figure 7.

h (cm) \ x (cm)	3·7	8·7	18·7	38·7	63·7	83·7
0·60	11·9	5·50	2·30	1·24	0·817	0·623
1·50	0·897	1·04	1·63	1·61	0·981	0·832
3·35	0·374	0·377	0·316	0·331	0·475	0·656

TABLE 1. Values of the wake parameter Π.

calculated from (4) in the manner described in § 3. The values of Π determined for each profile are listed in table 1. A remarkable point is that Π varies conspicuously with x and becomes closer to the value $0{\cdot}6 \sim 0{\cdot}7$ usually recommended for a constant-pressure boundary layer as x increases. Figure 11 indicates that the deformation of the velocity profile begins to decay with increasing x downstream from $x = 18{\cdot}7$ cm

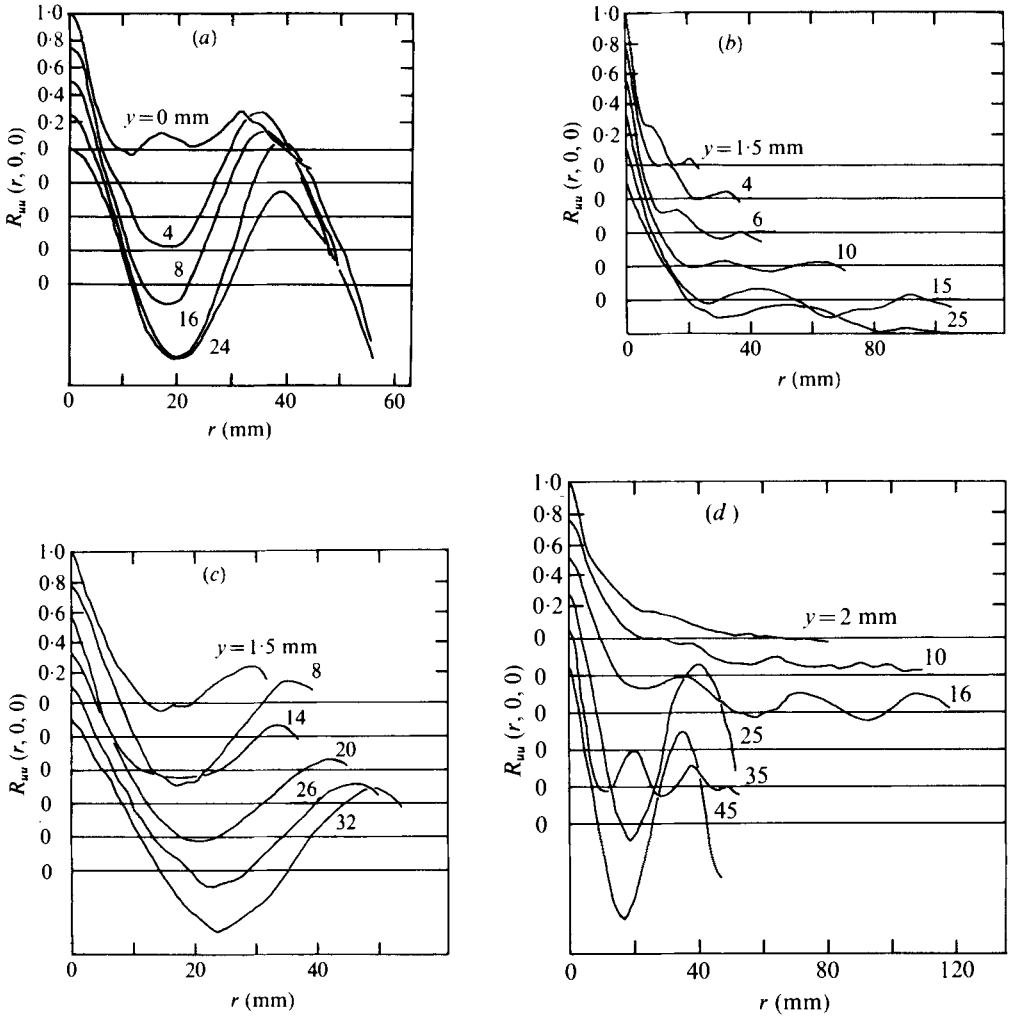

FIGURE 12. Transformed longitudinal correlation coefficients of u for the wake and the disturbed boundary layers at $x = 3{\cdot}7$ cm. (*a*) Isolated wake. (*b*) $h = 0{\cdot}60$ cm. (*c*) $h = 1{\cdot}50$ cm. (*d*) $h = 3{\cdot}35$ cm.

for each case. The decay rates are similar in each case. Figure 11 shows that the mean velocity field has almost recovered at $x = 83{\cdot}7$ cm, taking account of the fact that the reference velocity calculated in the present manner has a consistent discrepancy from the actual velocity even in the undisturbed case. On the other hand, table 1 shows that complete recovery of the mean velocity field has not been attained even at the last x station when $h = 1{\cdot}50$ cm. The value of Π at the last x station in the case $h = 3{\cdot}35$ cm gives the impression that the velocity field has almost completely recovered. But this value should be interpreted very carefully, because some detailed distortion remains.

Figures 12(*b*), (*c*) and (*d*) show the correlation coefficients obtained at $x = 3{\cdot}7$ cm for each case. In the case $h = 0{\cdot}60$ cm, the periodic component does not contribute so much to the intensity of the streamwise fluctuating velocity $\overline{u^2}$ at any height in

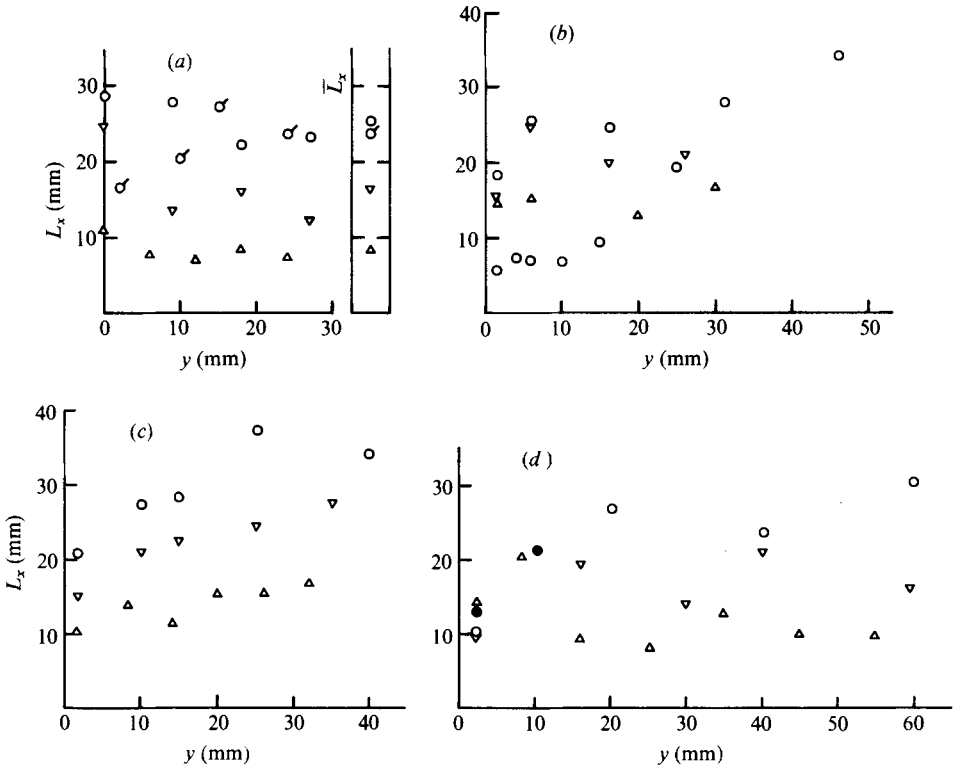

FIGURE 13. Distributions of integral scale L_x for the wake and the boundary layers. (*a*) Isolated wake and undisturbed boundary layer. (*b*) $h = 0{\cdot}60$ cm. (*c*) $h = 1{\cdot}50$ cm. (*d*) $h = 3{\cdot}35$ cm. ♂, undisturbed layer at $x = 0$; other symbols as in figure 7.

the boundary layer. Its most significant contribution is found at $y = 25$ mm and it may amount to 10% of $\overline{u^2}$ according to the simple evaluation mentioned in § 3. In comparison with this, the periodic component contributes comparably to $\overline{u^2}$ at all positions when $h = 1{\cdot}50$ cm. Even at $y = 1{\cdot}5$ mm, i.e. very close to the wall, its contribution may amount to 15%. For $h = 3{\cdot}35$ cm, on the other hand, the periodic component can hardly be detected near the wall but its contribution in the outer region is the largest. The periodic component of the fluctuation can be detected at $x = 18{\cdot}7$ cm when $h = 1{\cdot}50$ cm and even at $x = 38{\cdot}7$ cm when $h = 3{\cdot}35$ cm (data not shown here). In the case $h = 3{\cdot}35$ cm, however, the existence of a periodic component cannot be detected at the position nearest to the wall at any x station. In this case the Kármán-like vortices may disappear before the free shear layer reaches the wall. The frequency spectra obtained through on-line Fourier transformations of these correlations indicate that the fundamental frequencies of the periodic components are about 215 Hz, 250 Hz and 325 Hz for the cases $h = 0{\cdot}60$, $1{\cdot}50$ and $3{\cdot}35$ cm, respectively. The last frequency is the same as that found in the wake of a cylinder located in the free stream. Thus these periodic components are due to the Kármán-like vortex, whose discharge frequency is affected by the wall interaction or by the non-uniformity of the flow around the cylinder. This Kármán-like vortex persists for quite a large distance downstream from the cylinder when $h = 3{\cdot}35$ cm but never reaches the wall as mentioned above. In the case $h = 0{\cdot}60$ cm, it is not so strong initially and

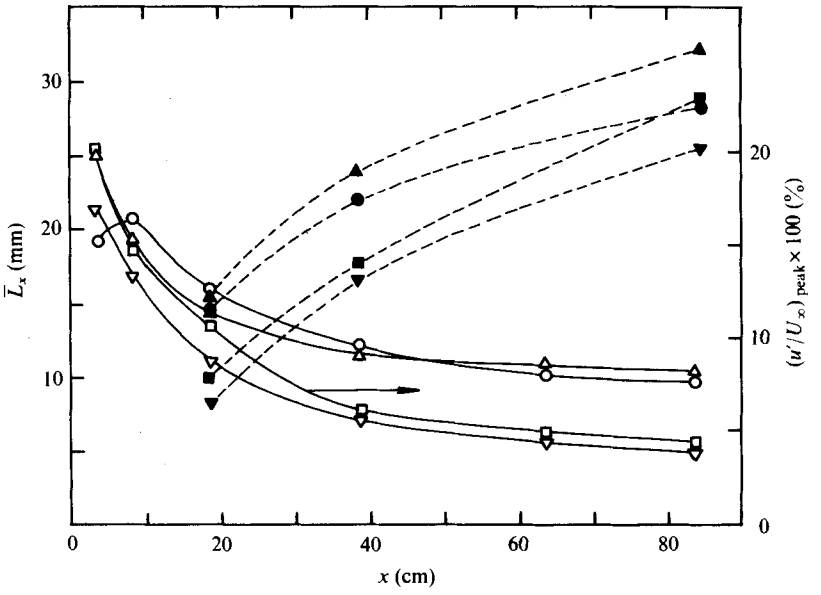

FIGURE 14. Variation of averaged integral scale and peak intensity with x. Symbols as in figure 8. Closed symbols, $\bar{L}_x$; open symbols, peak in u'/U_∞.

disappears rapidly, but its contribution to $\overline{u^2}$ is detectable near the wall at small x. Finally, it is strong over the whole thickness of the boundary layer when $h = 1{\cdot}50$ cm and does not disappear so rapidly as in the case $h = 0{\cdot}60$ cm.

The distributions of the integral scale across the boundary layer are shown in figures 13(*b*), (*c*) and (*d*) for several x positions. At $x = 18{\cdot}7$ cm it is observed that the integral length scale is smaller in the outer layer, in all cases, than that found in the outer layer at $x = 0$ in the undisturbed case. On the other hand, the results for $h = 3{\cdot}35$ cm at the two points nearest the wall are almost the same as those for the undisturbed case (shown in figure 13*a*) because the turbulence generated in the wake of cylinder has not yet reached these points. The result for $h = 0{\cdot}60$ cm at the point nearest the wall is almost the same as that for the undisturbed case but this may be due to a reason different from that for $h = 3{\cdot}35$ cm: the turbulence scale may have been restored from the disturbed value almost to that appropriate for a newly established wall shear layer with a logarithmic profile (figure 7). This may explain why the length scale for this case increases rapidly up to $x = 18{\cdot}7$ cm but remains at almost the same value afterwards. In the case $h = 1{\cdot}50$ cm, the length scale at the position near the wall at $x = 18{\cdot}7$ cm is much less than that in the undisturbed case and the trend of the variation of the length scale with x after that point is similar to that in the outer layer. The length scale averaged over the outer layer is denoted by $\bar{L}_x$ and is plotted in figure 14. The variation of $\bar{L}_x$ with x is much the same as that in the wake of a cylinder located in the free stream, also shown in the figure, but is different from that of the undisturbed boundary layer (which is not shown here but may be estimated from the variation of the boundary-layer thickness; see figure 8, keeping in mind that $\bar{L}_x$ in the undisturbed boundary layer is, as may be seen from figure 14 or 13(*a*), almost the same as the boundary-layer thickness). The ratios of the length scale to the boundary-layer thickness at $x = 18{\cdot}7$, $38{\cdot}7$ and $83{\cdot}7$ cm are $0{\cdot}44$, $0{\cdot}50$ and $0{\cdot}52$,

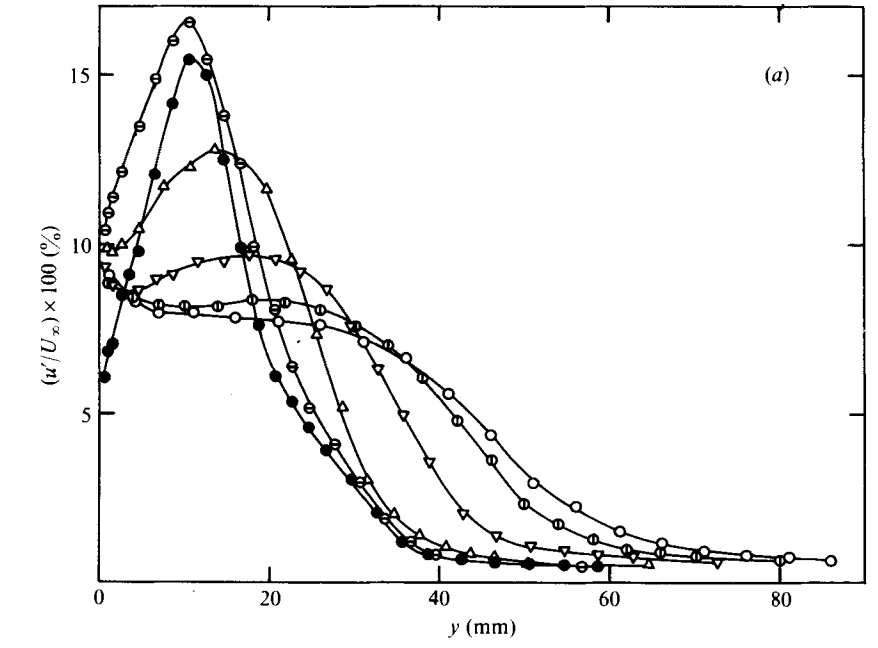

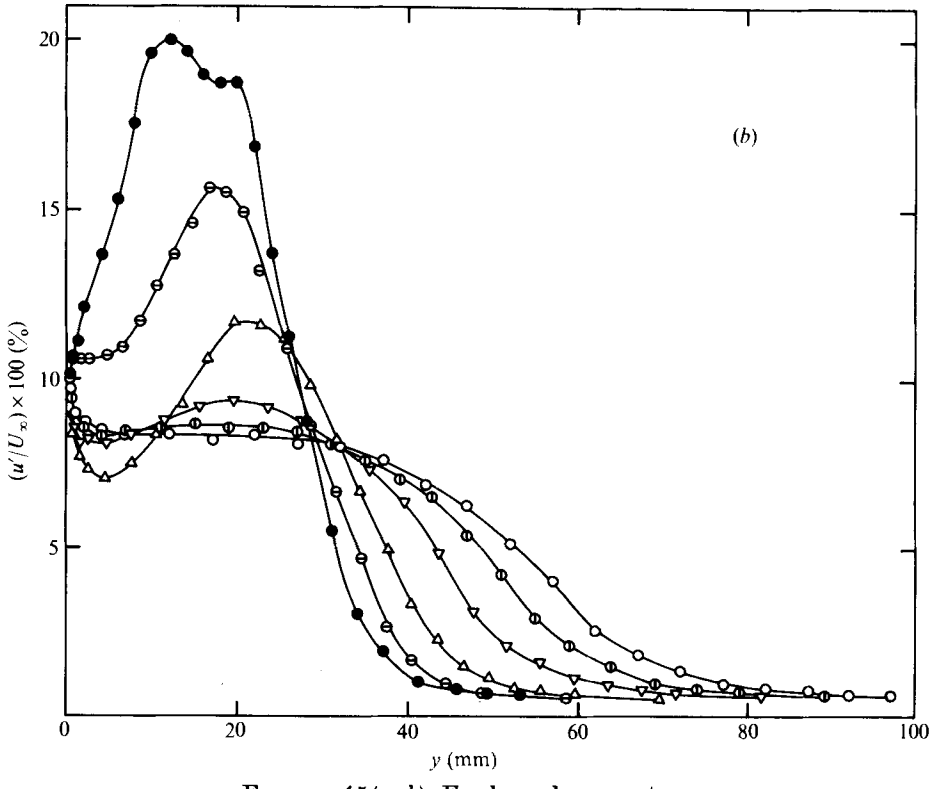

FIGURES 15(*a*, *b*). For legend see next page.

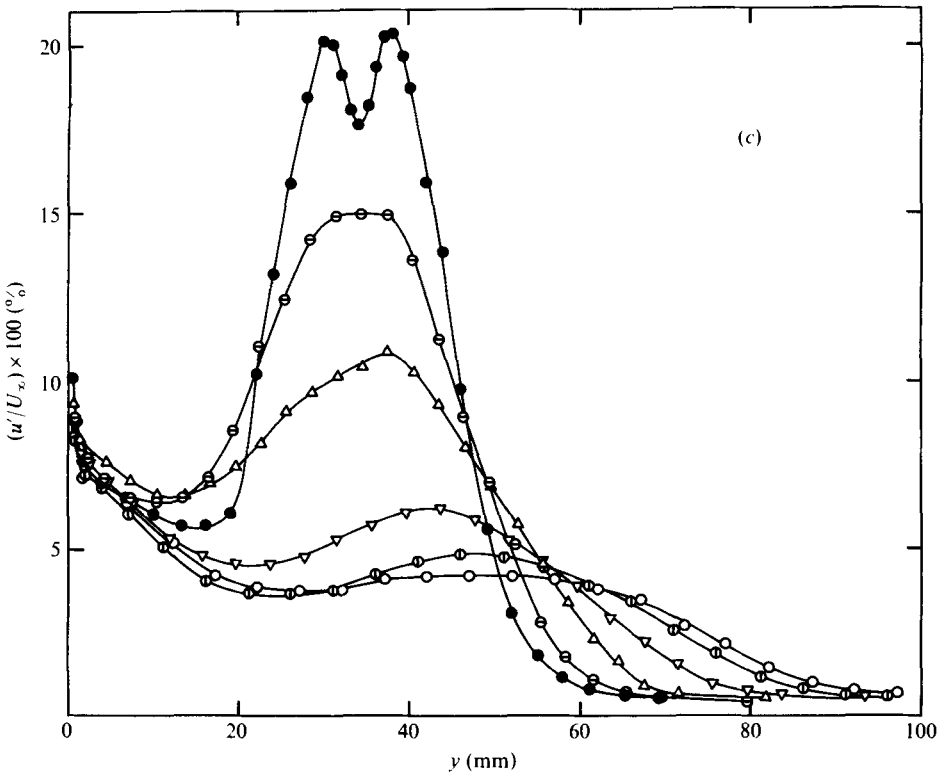

FIGURE 15. Distributions of longitudinal turbulence intensity for the disturbed boundary layers. (*a*) $h = 0{\cdot}60$ cm. (*b*) $h = 1{\cdot}50$ cm. (*c*) $h = 3{\cdot}35$ cm. Symbols as in figure 7.

respectively, for the case $h = 0{\cdot}60$ cm. Thus even at the largest x distance the turbulence is still far from equilibrium. The ratio $\bar{L}_x/\delta$ is 0·36, 0·48 and 0·53 for $h = 1{\cdot}50$ cm and 0·17, 0·30 and 0·37 for $h = 3{\cdot}35$ cm, respectively. The deviations of these ratios from unity for the undisturbed boundary layer are surprisingly large if we consider the fact that the mean-flow properties discussed above are comparatively close to equilibrium.

Figures 15(*a*), (*b*) and (*c*) show the distributions of the intensity of the streamwise fluctuating velocity in the boundary layer. It can be seen that the peak moves outwards somewhat rapidly with increasing x. This is due not to the mean motion of the fluid but mainly to the turbulent diffusion of the intensity of the fluctuating velocity. In any case the distributions at the last two x positions have the characteristic of a fairly flat profile in the middle of the boundary layer, which is a residue of the cylinder wake. Figure 14 shows also the streamwise variation of the peak intensity of the fluctuating velocity. The peak intensity is rather difficult to evaluate at large x. The values shown in the figure at these stations are values averaged over several points on the profile. The figure indicates that the variation of the intensity with x is very similar to that found in the wake of a cylinder, also shown in the figure, in the case $h = 3{\cdot}35$ cm. In the other two cases, the changes are more gradual. Comparing the latter two cases, the change in the case $h = 0{\cdot}60$ cm is rapid compared with that in the case $h = 1{\cdot}50$ cm. Figure 16 shows the non-dimensionalized thickness of the

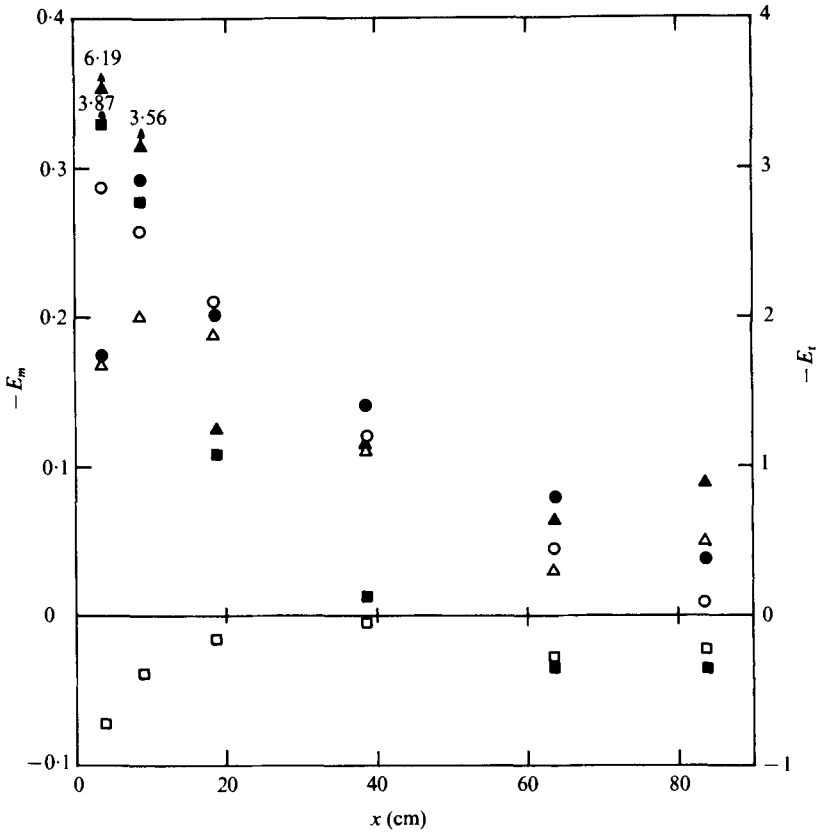

FIGURE 16. Variation of excess energy thicknesses for mean velocity and fluctuating velocity. ○, h = 0·60 cm; △, h = 1·50 cm; □, h = 3·35 cm. Open symbols, E_m; closed symbols, E_t.

excess kinetic energy for both the mean velocity and the fluctuating velocity. The thicknesses are defined as follows:

$$E_m = \int_0^1 (U^2 - U_{ud}^2)\, d\left(\frac{y}{\delta}\right) \Big/ \int_0^1 U_{ud}^2\, d\left(\frac{y}{\delta}\right), \tag{11}$$

$$E_t = \int_0^1 (\overline{u_{ud}^2} - \overline{u^2})\, d\left(\frac{y}{\delta}\right) \Big/ \int_0^1 \overline{u_{ud}^2}\, d\left(\frac{y}{\delta}\right), \tag{12}$$

where the suffix *ud* denotes the undisturbed boundary layer. It is seen that the mean-flow energy thickness E_m is much smaller than the turbulence energy thickness E_t if the comparison is made at the same location. This means that the disturbance of the mean flow is much smaller than that of the turbulence field and is restored rather rapidly. The fact that the turbulence field does not recover so fast has been already observed in the variation of the turbulence length scale with x. The variation of E_t when h = 1·50 cm is gradual compared with the case h = 0·60 cm, cf. the gradual variation of the peak intensity shown in figure 14. The variation of E_t for the case h = 3·35 cm is different from that in the other two cases: in this case, the turbulence kinetic-energy thickness is smaller than in the undisturbed case. Even at x = 83·7 cm, the turbulence kinetic-energy thickness is far from zero. This is because the turbulence

intensity in the outer layer at the last x station is lower than that in the undisturbed case. This means that the properties of the turbulence in this region closely resemble those of wake turbulence, as may be seen from the intensity decay rate shown in figure 14. Thus the turbulence kinetic-energy thickness may not approach zero before the wall turbulence is redistributed after $x = 83{\cdot}7$ cm over the entire region of the outer layer. Even when $h = 0{\cdot}60$ cm, the length scale found in the outer layer at $x = 83{\cdot}7$ cm is much smaller than that in the undisturbed boundary layer. These facts suggest that it takes a fairly long additional distance for the turbulence intensity profile in the boundary layer to recover completely, not only when $h = 3{\cdot}35$ cm but also in the other two cases. This again indicates that the turbulence field recovers more slowly than the mean velocity field.

5. Conclusions

A turbulent boundary layer disturbed by a cylinder exhibits different behaviour according to the position of the cylinder. The main conclusions obtained from the experiment are as follows.

(i) The friction coefficient c_f increases rapidly from near zero and approaches the value for an undisturbed boundary layer when $h = 0{\cdot}60$ cm ($h/\delta_0 = 0{\cdot}222$). When $h = 1{\cdot}50$ cm ($h/\delta_0 = 0{\cdot}556$) it decreases initially then begins to increase at a point downstream from the cylinder, whereas when $h = 3{\cdot}35$ cm ($h/\delta_0 = 1{\cdot}24$) it initially maintains an almost constant value then decreases slowly after $x = 40$ cm. These trends can be understood by considering both the change in the flow pattern and the arrival of cylinder-wake turbulence in the near-wall region.

(ii) These variations of c_f can be roughly predicted by the equations given by Ludwieg & Tillmann and Escudier *et al.*

(iii) The disturbed boundary layers recover faster in the near-wall region than in the outer region and the logarithmic part of the velocity distributions reappears only a short distance downstream of the cylinder.

(iv) The quantities defined by (11) and (12) represent well the restoration rates of the mean and turbulent kinetic energy and make it easy to compare the restorations to equilibrium of two flow fields. The results show that the fluctuating field returns to equilibrium more slowly than the mean flow field does.

(v) The boundary layer appears to return to equilibrium faster in the case when $h = 0{\cdot}60$ cm than in the other cases.

(vi) The relation between H_{32} and H_{12} obtained from the measurements accords with the equation given by Nicoll & Escudier.

(vii) The characteristics of the outer-layer turbulence are very similar to those of wake turbulence and for this reason the entrainment rate of the fluid is almost the same as that for a wake.

(viii) Strong periodicity of the fluctuating velocity is found at $x = 3{\cdot}7$ cm when $h = 1{\cdot}50$ and $3{\cdot}35$ cm, but the periodic fluctuation is not so intense when $h = 0{\cdot}60$ cm.

REFERENCES

ANTONIA, R. A. & LUXTON, R. E. 1972 *J. Fluid Mech.* **53**, 737.

BRADSHAW, P. & WONG, F. Y. F. 1972 *J. Fluid Mech.* **52**, 113.

CLAUSER, F. H. 1956 *Adv. Appl. Mech.* **4**, 1.

COLES, D. E. 1968 *AFOSR–IFP–Stanford Conf. Comp. Turbulent Boundary Layers, Stanford Univ.* vol. 2, p. 5.

ESCUDIER, M. P., NICOLL, W. B. & SPALDING, D. B. 1966 *Dept. Mech. Engng, Imp. Coll. Tech. Note* TWF/TN/12.

ESKINAZI, S. 1958 *N.A.S.A. Tech. Note* D-83.

FUJITA, H., TAKAHAMA, H. & YAMASHITA, R. 1974 *Proc. 11th Japan Heat Transfer Symp., Nagoya*, p. 453.

HINZE, J. O., SONNENBERG, R. E. & BUILTJES, P. J. H. 1974 *Appl. Sci. Res.* **29**, 1.

IRWIN, H. P. A. H. 1974 *Aero. Res. Counc. Current Paper* no. 1267.

KACKER, S. C. & WHITELAW, J. H. 1968 *Trans. A.S.M.E., J. Appl. Mech.* E **90**, 641.

KACKER, S. C. & WHITELAW, J. H. 1971 *Trans. A.S.M.E., J. Appl. Mech.* E **93**, 239.

KLEBANOFF, P. S. 1954 *N.A.C.A. Tech. Note* no. 3178.

LUDWIEG, H. & TILLMANN, W. 1950 *N.A.C.A. Tech. Memo.* no. 1285.

NICOLL, W. B. & ESCUDIER, M. P. 1966 *A.I.A.A. J.* **4**, 940.

PATEL, V. C. 1965 *J. Fluid Mech.* **23**, 185.

REICHARDT, H. 1942 *VDI-Forchungsheft*, p. 414.

SCHLICHTING, H. 1930 *Ing. Arch.* **1**, 533.

SCHLICHTING, H. 1968 *Boundary Layer Theory*. McGraw-Hill.

TANI, I. 1968 *AFOSR–IFP–Stanford Conf. Comp. Turbulent Boundary Layers, Stanford Univ.* vol. 1, p. 483.